Comparative Analysis of feature extraction (2D FFT & Wavelet) and classification (L_p metric distances, MLP NN, & HNeT) algorithms for SAR imagery

Nicholas Sandirasegaram and Ryan English
Defence R&D Canada – Ottawa, Ottawa, ON, K1A 0Z4, Canada

ABSTRACT

The performance of several combinations of feature extraction and target classification algorithms is analyzed for Synthetic Aperture Radar (SAR) imagery using the standard Moving and Stationary Target Acquisition and Recognition (MSTAR) evaluation method. For feature extraction, 2D Fast Fourier Transform (FFT) is used to extract Fourier coefficients (frequency information) while 2D wavelet decomposition is used to extract wavelet coefficients (time-frequency information), from which subsets of characteristic in-class "invariant" coefficients are developed. Confusion matrices and Receiver Operating Characteristic (ROC) curves are used to evaluate and compare combinations of these characteristic coefficients with several classification methods, including L_p metric distances, a Multi Layer Perceptron (MLP) Neural Network (NN) and AND Corporation's Holographic Neural Technology (HNeT) classifier. The evaluation method examines the trade-off between correct detection rate and false alarm rate for each combination of feature-classifier systems. It also measures correct classification, misclassification and rejection rates for a 90% detection rate. Our analysis demonstrates the importance of feature and classifier selection in accurately classifying new target images.

Keywords: Synthetic Aperture Radar (SAR), Feature extraction, Classification, FFT, Wavelet, MLP, HNeT, Neural Network, ROC, Confusion matrix.

1.0 INTRODUCTION

In recent years, the research community has increased the use of SAR imagery in ATR development [1,2,3]. SAR ATR systems, however, are still in the developmental stage and it will be some time until they are fully operational. A SAR-based ATR system requires a fast and effective discriminator to detect a target and recognize the type of target from radar return [4]. This study concentrates on the target recognition process. The target recognition process as illustrated in Figure 1, can be broken into meaningful processing steps: detection, preprocessing, feature extraction and classification.

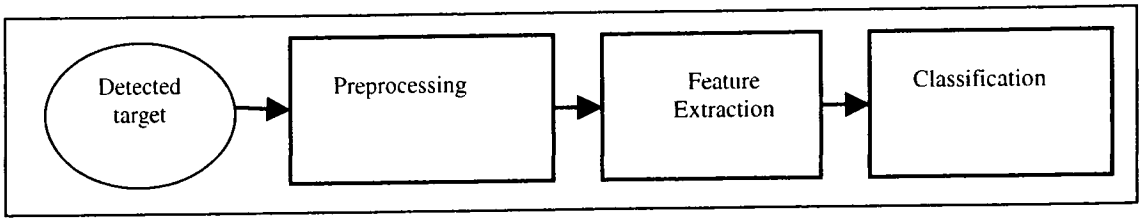

Figure 1: Block diagram of target recognition processing steps.

In this study, various algorithms were applied in the feature extraction and classification steps and then their performance compared. Two Dimensional Fast Fourier Transform (2D FFT) and Two Dimensional Wavelet Transform (WT) were applied to extract significant features in SAR images.

Algorithms for Synthetic Aperture Radar Imagery XII, edited by Edmund G. Zelnio, Frederick D. Garber, Proceedings of SPIE Vol. 5808 (SPIE, Bellingham, WA, 2005) 0277-786X/05/$15 · doi: 10.1117/12.597305

These 2D FFT [5-7] and WT [8,9] algorithms were used successfully in SAR ATR application. Three different classification algorithms; Multi Layer Perceptron (MLP) Neural Network (NN), AND Corporation's Holographic Neural Technology (HNeT) and L_p metric distances classifiers were evaluated and compared. The MLP NN method is already used in many applications; character recognition [10,11,12], data mining [13,14] and ATR [5,15] applications. HNeT is a commercial software of the AND Corporation and it is implemented based on Artificial Neural Network technology [16,17,18]. The HNeT is applied in various applications, including face recognition [19,20] and ATR [6,21] applications. The L_p metric distance is a simple classifier, which measures the dissimilarity between two sets of target features. This L_p method is applied in pattern recognition [22,23]. Euclidean metric distance (L_2) is used in this paper and this method is a special case of the L_p family (p=2).

The data set that is used here is from the Moving and Stationary Target Acquisition and Recognition (MSTAR) data set, which is available to the public [24]. The MSTAR public data set contains many spotlight SAR vehicle images including 10 types of former Soviet Union vehicles with 0 to 360 degrees azimuthal angle and the depression angles of 15 and 17degrees. The COMPASE Center of AFRL developed a standard MSTAR evaluation methodology to evaluate the ATR algorithms using the MSTAR public data set [25]. The standard evaluation method uses Confusion Matrix and Receiver Operating Characteristic (ROC) curves to evaluate the algorithms and has been applied to the other ATR algorithms [6,26,27]. Here this method is also used to evaluate and compare the features and classifiers.

2.0 DETECTED TARGET

The concept of detection is meaningful when information about objects of interest account for only a small fraction of the data being considered. For SAR imagery, this is typical when a few vehicles, for instance, with dimensions of meters are the targets of interest within a scene having dimensions of kilometers. Target detection, therefore, provides location information about points or regions of interest within a scene. Once a list of target detections is compiled, it is desirable to isolate each detection and apply the same ATR process to each of them independently.

Typically, a subimage, referred to as a chip, is extracted so that each chip contains one complete target. Chips are usually standardized in size, large enough to contain the dimensions of the largest target, but not so large as to include objects other than the target. The target chips for this investigation come from the MSTAR public data set of former Soviet armored vehicles. Each chip is 128 pixels by 128 pixels with a pixel spacing of 0.20 meters.

3.0 PREPROCESSING

Some feature extraction algorithms and classification algorithms are sensitive to location shift, rotation, and non-uniform illumination. Reducing the sensitivity to these geometric and radiometric variations can enhance the accuracy of an ATR system. In this paper, only the value of magnitude was considered and the phase information ignored. All the target chips (training and testing) were converted from slant-range to ground-range. In the MSTAR dataset the target contained within each chip is oriented independently of the other chips. To bring the targets into a standardized target orientation, each target was rotated to a vertical orientation. For this rotation, the orientation angle is found using ground truthing information.

After rotating to the standardized orientation, the highest energy reflecting point of the target is found in the target chip. A median filter is applied to isolate the target region in the target chip, and a search is subsequently used to locate the highest energy return point in that region. The energy at this point represents the highest energy reflected towards the radar sensor for particular sensor depression angle and target orientation. This point of highest energy is then used as the centre point for a new chip, the

size of which 64 pixels by 64 pixels. The reduced size of the new target chip is more than enough to cover any target (not shadow) in the MSTAR 3 target problem.

The final preprocessing step is to normalize the target chips. Normalization alters the pixel values such that, the mean intensity is zero and the standard deviation value is one for each chip. The mathematical explanation is given by the following equation.

$$f(i,j)=\frac{X(i,j)-\overline{X}}{\sigma_X},\quad 1\le i\le N, 1\le j\le M, \tag{1}$$

where X is the non-normalized target chip, f is the normalized target chip, $\overline{X}$ is the mean pixel intensity of the target chip X, σ_x is standard deviation (pixel intensity) of the target chip X, N is the number of pixels in the range direction, and M is the number of pixels in the cross range direction. The normalized target chip is then passed on to feature extraction algorithms.

4.0 FEATURE EXTRACTION METHODS

Feature extraction is the most important steps in the ATR process. Feature extraction algorithms extract unique information or a signature from each target. A very good feature extraction algorithm gives smaller variation between the same type of targets and larger variation between different types of targets. Selection of a good feature extraction algorithm is important; otherwise, it will be difficult to differentiate between targets of different types and misclassification will occur. 2D FFT feature extraction and 2D WT feature extraction methods were applied for this study. 2D FFT was applied to targets, which were weighted by four different window functions. Similarly, 2D WT transform was applied to targets using four different mother wavelets. These different window functions and mother wavelets effects in classification were compared at result and discussion section.

4.1 Two Dimensional Fast Fourier Transform Method

The 2D Fourier analysis gives the frequency response of an image/target and depends on the periodic components that occur in the target. Features are selected based on these dominant periodic components in each target types. Four different 2D window-weighting functions were applied to the target before the 2D FFT. The considered four 2D window functions were constructed from one dimensional functions [28] as given below

$$w_c(n_1,n_2) = w_1(n_1)^T\, w_2(n_2), \text{ where } n_1=0,2,\ldots N\text{-}1 \text{ and } n_2=0,2,\ldots M\text{-}1 \tag{2}$$

where w_1 and w_2 are one dimensional window functions in mutually perpendicular directions and $w_c(n_1,n_2)$ is the two dimensional "c" window function, which in 1D forms [29,30] are listed below. In this study, window lengths in both directions are selected to be equal, M = N = 64.

i) Rectangular
$$w_{Rec1}(n_1) = 1,\quad w_{Rec2}(n_2) = 1, \tag{3}$$

ii) Hanning
$$w_{Han1}(n_1) = 0.5\,(1-\cos(2\pi n_1/(N\text{-}1))),\quad w_{Han2}(n_2) = 0.5\,(1-\cos(2\pi n_2/(N\text{-}1))) \tag{4}$$

iii) Hamming
$$W_{Ham1}(n_1) = 0.54-0.46\cos(2\pi n_1/(N\text{-}1)),\quad W_{Ham2}(n_2) = 0.54-0.46\cos(2\pi n_2/(N\text{-}1)) \tag{5}$$

iv) Blackman
$$W_{Bla1}(n_1) = 0.42-0.5\cos(2\pi\, n_1/(N\text{-}1))+0.08\cos(4\pi\, n_1/(N\text{-}1)),\quad W_{Bla2}(n_2) = 0.42-0.5\cos(2\pi n_2/(N\text{-}1))+0.08\cos(4\pi n_2/(N\text{-}1)) \tag{6}$$

Each target was weighted using the above 2D window functions, that is, simple pixel-to-pixel multiplication in space domain.

$$y_c(n_1,n_2) = w_c(n_1,n_2)f(n_1,n_2) \tag{7}$$

where $f(n_1, n_2)$ is the normalized target image (eq. 1), $y_c(n_1, n_2)$ is the weighted image weighted by the "c" 2D window function. Then, 2D FFT was applied (see equation 8) to the weighted target and extracted 2D Fourier coefficients.

$$Y_c(u_1,u_2) = \frac{1}{N} \sum_{n_1,n_2=0}^{N-1} y_c(n_1,n_2)\, e^{-j\frac{2\pi}{N}(n_1u_1+n_2u_2)} \tag{8}$$

where $Y_c(u_1,u_2)$ are the 2D Fourier coefficients. Only half of the coefficients are unique due to symmetry. These coefficients are complex, so the magnitude of these coefficients is taken for use in this study. Some of these coefficients are relatively invariant around the same type of target and some of them take on random values for the same type of target. It is important to discriminate invariant coefficients from random coefficients. As applied in previous work [5], dominant features' (coefficients') locations were located by coherently combined the coefficients of the same type of targets with other target types and non-targets. A total of 24 dominant coefficients were selected for the comparison. Each of the three target types (BMP2, BTR70, and T72) is considered independently in this problem, so exactly 24 features were used for each of the target types.

4.2 Two Dimensional Wavelet Transform Method

The 2D WT decomposes the original image into several sub images of coarser resolutions than the original image. At each level of decomposition, four sub images (LL, LH, HL, HH) are obtained according to the mother wavelet function. LL contains low frequency components in horizontal and vertical directions. LH contains low frequency components in horizontal direction and high frequency components in vertical direction. HL contains high frequency components in horizontal direction and low frequency components in vertical direction. HH contains high frequency components in both horizontal and vertical directions.

Fourier analysis expresses the original image in terms of a sum of basis functions. These basis functions are sinusoids of different frequencies. Similarly, the wavelet analysis expresses the original image in terms of sum of basis functions, but these basis functions are shifted and scaled versions of mother wavelet. Here, we consider only separable 2D WT. Because 2D WT can be computed using 1D scaling and wavelet functions.

The 2D WT decomposes an image in terms of wavelet and scaling functions [31]. The following equation shows the 2D wavelet decomposition of an image $f(n_1,n_2)$, $f(n) \in L^2(\Re)$.

$$f(n) = \sum_{k\in Z^2} a_{j0,k}\, \phi^{LL}_{j0,k}(n) + \sum_{b\in B} \sum_{j\geq j0} \sum_{k\in Z^2} d^b_{j,k}\, \psi^b_{j,k}(n), \tag{9}$$

where $b \in B := \{LH, HL, HH\}$, $\phi^{LL}_{j0,k}(n)$ is the 2D dilated and translated scaling function, a_{j0} are the scaling or approximation coefficients, $\psi^b_{j,k}$ is the 2D translated and dilated wavelet function, $d^b_{j,k}$ are the detail or wavelet coefficients, j ($j \geq j_0$) is a scale factor, k (two dimensional variable $k=(k_1,k_2)$) is the shifting factor of the wavelet and scale functions, respectively, and j_0 is a fixed scale. These 2D functions can be broken down into the product of 1D functions [31, 32].

$$\phi^{LL}_{j0,k}(n) = \phi_{j0,k1}(n_1)\,\phi_{j0,k2}(n_2) \tag{10}$$

$$\psi^{LH}_{j,k}(n) = \psi_{j,k1}(n_1)\,\phi_{j0,k2}(n_2) \tag{11}$$

$$\psi^{HL}_{j,k}(n) = \phi_{j0,k1}(n_1)\,\psi_{j,k2}(n_2) \tag{12}$$

$$\psi^{HH}_{j,k}(n) = \psi_{j,k1}(n_1)\,\psi_{j,k2}(n_2) \tag{13}$$

where $\phi_{j0,k1}(n_1)$ and $\psi_{j,k1}(n_1)$ are the 1D column direction scaling and wavelet functions, and $\phi_{j0,k2}(n_2)$ and $\psi_{j,k2}(n_2)$ are the 1D row direction scaling and wavelet functions. These 1D translated and dilated functions form the mother wavelet and scaling functions:

$$\phi_{j0,n}(t) = 2^{j0/2}\phi(2^{j0}t - m), \tag{14}$$

$$\psi_{j,n}(t) = 2^{j/2}\psi(2^{j}t - m),\ m = k_1, k_2 \text{ and } t = n_1, n_2, \tag{15}$$

where ϕ is the mother scaling function and the ψ is the mother wavelet function. The approximation coefficients $a_{j0,k}$ and the detail coefficients $d^{b}_{j,k}$ can be found using the following equations [33] in discrete form.

$$a_{j0,(k1,k2)} = \sum_{u1}\sum_{u2} f(n_1, n_2)\,\phi_{j0,k1}(n_1)\,\phi_{j0,k2}(n_2) \Rightarrow LL \tag{16}$$

$$d^{LH}_{j,(k1,k2)} = \sum_{u1}\sum_{u2} f(n_1, n_2)\,\psi_{j,k1}(n_1)\,\phi_{j0,k2}(n_2) \Rightarrow LH \tag{17}$$

$$d^{HL}_{j,(k1,k2)} = \sum_{u1}\sum_{u2} f(n_1, n_2)\,\phi_{j0,k1}(n_1)\,\psi_{j,k2}(n_2) \Rightarrow HL \tag{18}$$

$$d^{HH}_{j,(k1,k2)} = \sum_{u1}\sum_{u2} f(n_1, n_2)\,\psi_{j,k1}(n_1)\,\psi_{j,k2}(n_2) \Rightarrow HH \tag{19}$$

The 2D approximation and detail coefficients can be calculated from the 1D scaling and wavelet functions. This separable 2D discrete wavelet transform can be computed by applying the 1D low-pass and the high-pass digital filters [31-34] to an image $f(n_1,n_2)$. The low-pass filter represents the scaling function and high-pass filter represents the wavelet function [35]. This decomposition using 1D filters is achieved by first filtering the rows of the input image with the low pass and high pass filters and decimating the result by 2. The columns of the two decimated images are then filtered with the low and high pass filters and are subsequently decimated by 2 again. This first-level decomposition produces the four filtered images discussed above: LL, LH, HL, and HH. Then the LL detail coefficients are used for second level decomposition and it will produce another four filtered images.

The Matlab wavelet toolbox is used to extract these second level approximation image [36]. The sub-band image block diagram and an example illustration the 2D WT decomposition are shown in Figure 2. LL and LLLL are level 1 and level 2 approximation images. LH, HL and HH are the level 1 detail images, and LLLH, LLHL and LLHH are the level 2 detail images. The level 2 approximation image contains low frequency information in both the vertical and horizontal directions. That is, high frequency noise is removed in LLLL. In this study, the level 2 approximation sub-band image (LLLL) is considered for the target features. The same method as in section 4.1 was applied to extract 24 dominant features for each of the target types. Four different mother wavelets were applied to extract the second level approximation image, namely Coiflets, Daubechies, Reverse biorthogonal and Symlets wavelets.

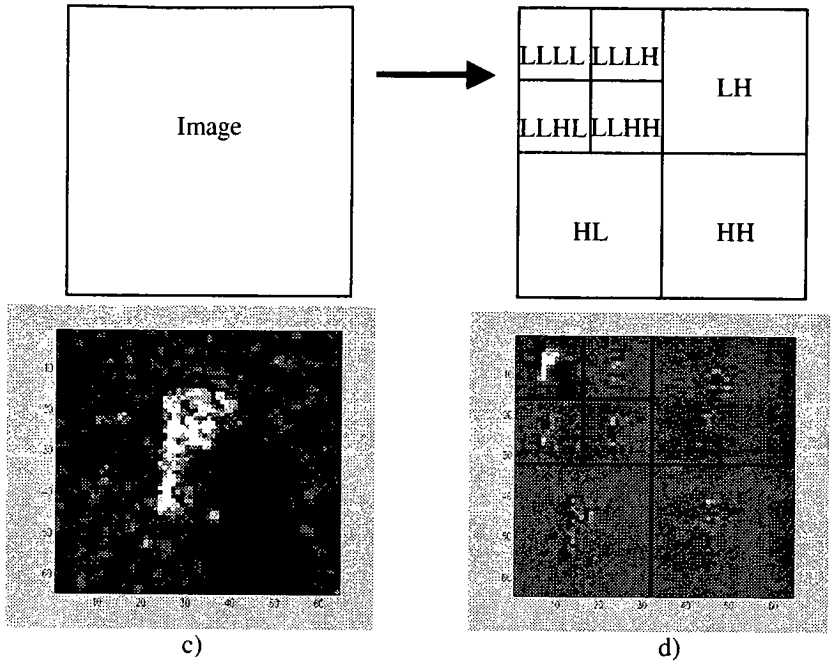

Figure 2: Two levels decomposition of discrete wavelet transform. a) Block representation of an image. b) Block Wavelet representation of second resolution levels. c) Original BMP-2 image. d) The BMP-2 Wavelet representation of second resolution levels.

5.0 CLASSIFICATION METHODS

Using the vector of extracted features, the classifier must be able to correctly decide whether each image is a known target or an unknown target. There are many classifier exists and each of them has their own strengths and weaknesses. Three classifiers were considered in this study and they are Euclidean metric measure (L_2), MLP NN, HNeT. All these classifiers were treated as binary classifiers except L_2 classifier.

5.1 Euclidean Metric Measure (L_2)

The Euclidean metric measure classifier is a special case of the L_p metric measure classifier whereby p=2. The L_2, $E(T^s,F)$ was computed as

$$E(T^s, F) = \sqrt{\sum_{i=1}^{P} (T_i^s - F_i)^2} \tag{20}$$

where P is number of features (in this study, P=24), T^s is the template s and F is the testing target. The template is created for each training target. The $E(T^s,F)$ distance shows the similarity between testing target and the matching template. Wide distance means that dissimilarity is high and short distance means that the similarity is high. It has following properties; positively, reflectivity, triangle inequality and symmetry.

5.2 Multi Layer Perceptron Neural Network

The most commonly used nonlinear regression model is the MLP NN, which is capable of learning nonlinear function mappings. It uses supervised learning method to learn about targets from their features. Standard delta rule back propagation algorithm is used for training the NN. During the learning phase, the NN learns the relationship between the information given at the input and the information requested from the output. In the responding phase, test data similar to the learning input data is fed to the input. Based on the learned response the NN then predicts the response to the test data. The MLP NN was configured with 15 nodes in the first hidden layer, 13 nodes in the second hidden layer, 24 nodes in the input layer and 2 nodes in the output layer.

5.3 Holographic Neural Technology (HNeT)

The HNeT is AND Corporation's commercial software and the classifier is implemented based on artificial NN technology. It uses supervised training method to map input features into a complex domain and searches for in-class invariance of those features within the training data. Further technical information about the HNeT classifier can be found in the references [16,37-41].

In this study, the HNeT classifier is used without applying the built-in feature extraction algorithms (no signal conversion), relying instead on the feature vectors generated externally, as used by the other classifiers.

6.0 RESULTS AND DISCUSSION

Several feature extraction processes were applied to the preprocessed images. Four different windowing functions applied independently to the preprocessed images before extracting the Fourier coefficients and four different mother wavelets applied independently to the preprocessed images to extract wavelet features. Therefore, eight independent feature sets were prepared and three different classifiers used these feature sets independently for classifying the three types of MSTAR targets.

All the training targets are listed on table 1 and tested targets are listed in table 2. The L_2 classifier uses the BMP-2, T-72 and BTR-70 types individually (Not the confusers) for creating templates.

Table 1. Training Set

Targets type and serial number	# of samples	Depression Angle
T-72 (132)	232	17^0
BTR-70 (c71)	233	17^0
BMP-2 (c21)	233	17^0
SLICY (Confusers)	274	15^0
Total	= 972	

Table 2. Testing set - Testing samples and confusers

Targets type and serial number	# of samples	Depression Angle
T-72 (812)	195	15^0
T-72 (s7)	191	15^0
T-72 (132)	196	15^0
BTR-70 (c71)	196	15^0
BMP-2 (c21)	196	15^0
BMP-2 (9566)	196	15^0
BMP-2 (9563)	195	15^0
2S1(Confusers)	274	15^0
D7 (Confusers)	274	15^0
Total	= 1913	

The feature comparison is done for each target type separately. ROC curves are plotted for each target type using three different classifiers. For generating ROC curves, the percentage of false alarm (P_f) was calculated using confusers listed in Table 2. The MLP NN classifier-based comparison is shown in Figure 3. As in [25,26], the region around where the percentage of declarations (P_d) crosses 0.9 is of particular interest. Therefore, this region is zoomed and placed in the lower part of the graph. For a clear view of the content, each feature name is abbreviated in the graph to Coi = Coiflets wavelet, Dau = Daubechies wavelet, Rev = Reverse biorthogonal wavelet, Sym = Symlets wavelet, Rec = Rectangular window, Ham = Hamming window, Han = Hanning window, and Bla = Blackman window. At the 0.9 P_d, the Hamming and Hanning windows, 2D FFT show low P_f for the T-72 and BMP2 target types compared to other features. For the BTR-70, all features show significantly better performance due to the single BTR vehicle available for testing is the same one used for training (at different depression angle). Here, the Reverse biorthogonal wavelet was the top performer.

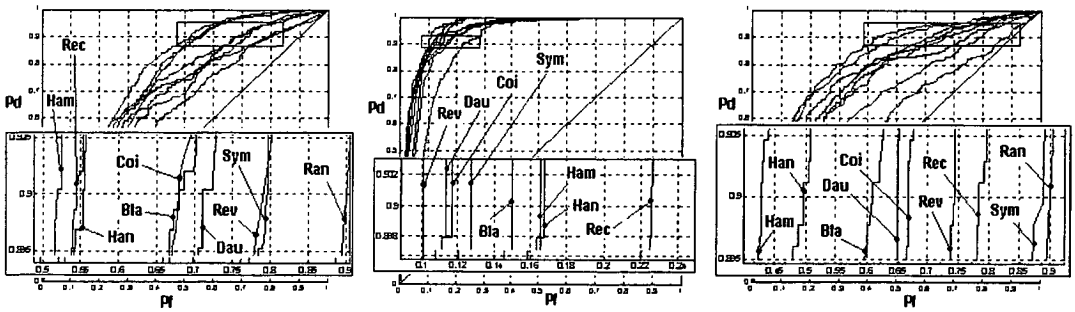

a) T-72 classification ROC curve b) BTR-70 classification ROC curves c) BMP-2 classification ROC curves

Figure 3: Feature Comparison using MLP NN

In comparing the features using HNeT classifier (Figure 4), a clear split occurs for the T-72 and BMP-2 results, with the Hamming, Hanning, Blackman and Rectangular windows forming a cluster outperforming the others at Pd = 0.9.

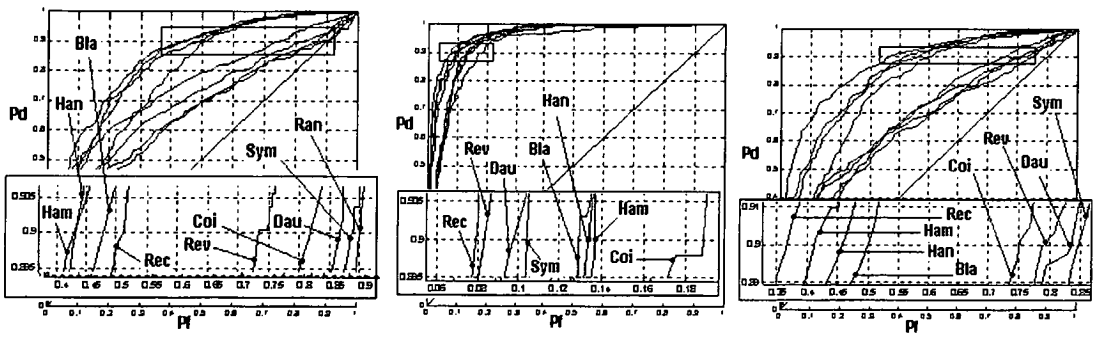

a) T-72 classification ROC curve b) BTR-70 classification ROC curves c) BMP-2 classification ROC curves

Figure 4: Feature Comparison using HNeT.

The third comparison was achieved using L_2 Metric Measure method and the results are shown in Figure 5. The Rectangular based classification yields the best results for the T-72 and BMP2 target types, and is only outperformed by the Reverse biorthogonal for the BTR-70.

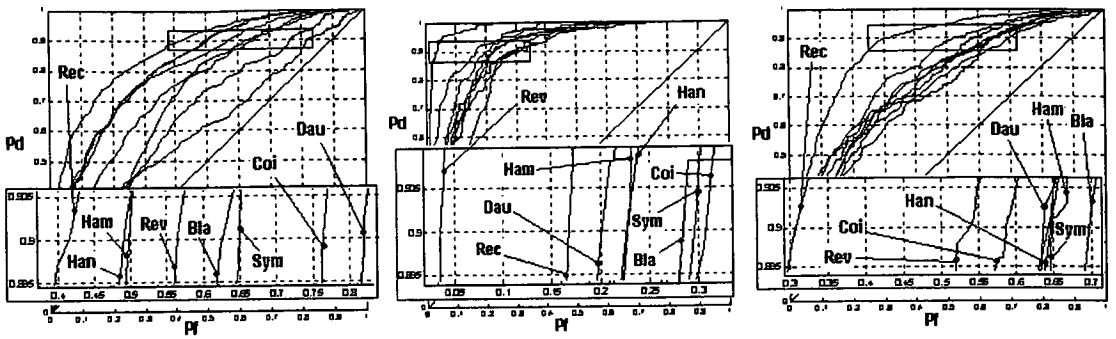

a) T-72 classification ROC curve b) BTR-70 classification ROC curves c) BMP-2 classification ROC curves

Figure 5: Feature Comparison using L_2.

Across target types, the Hamming, Rectangular and Hanning are solid performers across all three classifiers. For the BTR70 target type, the Reverse biorthogonal feature performed best for the L_2 and MLP NN classifiers, and the performance was second best when it was used with HNeT. The results are not clear for the BMP-2 target type. The Hamming and Hanning features perform well for the MLP NN and HNeT but not for the L_2. The Rectangular window shows good result with the L_2 and HNeT, but not for the MLP NN.

Table 3. Summary from the confusion matrices at 0.9 P_d

Feature	Each Type	MLP			HNeT			Lp		
		T72	BTR70	BMP2	T72	BTR70	BMP2	T72	BTR70	BMP2
Coi		Over all Pcc/d = 0.757			Over all Pcc/d =0.797			Over all Pcc/d =0.570		
	Pcc/d	0.633	0.894	0.821	0.795	0.845	0.784	0.611	0.393	0.593
	Pd	0.847	0.959	0.934	0.907	0.888	0.898	0.844	0.934	0.945
Dau		Over all Pcc/d =0.730			Over all Pcc/d =0.775			Over all Pcc/d =0.512		
	Pcc/d	0.598	0.862	0.809	0.751	0.837	0.779	0.660	0.103	0.496
	Pd	0.873	0.959	0.908	0.905	0.908	0.893	0.916	0.888	0.889
Rev		Over all Pcc/d =0.719			Over all Pcc/d =0.827			Over all Pcc/d =0.577		
	Pcc/d	0.606	0.755	0.815	0.810	0.847	0.837	0.527	0.324	0.715
	Pd	0.873	0.980	0.901	0.902	0.969	0.876	0.930	0.883	0.879
Sym		Over all Pcc/d =0.714			Over all Pcc/d =0.785			Over all Pcc/d =0.579		
	Pcc/d	0.637	0.865	0.735	0.801	0.840	0.749	0.568	0.289	0.686
	Pd	0.880	0.980	0.899	0.923	0.893	0.882	0.923	0.883	0.889
Rec		Over all Pcc/d =0.890			Over all Pcc/d =0.909			Over all Pcc/d =0.854		
	Pcc/d	0.874	0.977	0.878	0.907	0.970	0.891	0.886	0.858	0.823
	Pd	0.967	0.888	0.838	0.905	0.857	0.910	0.888	0.898	0.913
Ham		Over all Pcc/d =0.907			Over all Pcc/d =0.926			Over all Pcc/d =0.804		
	Pcc/d	0.922	0.972	0.868	0.910	0.977	0.925	0.712	0.869	0.873
	Pd	0.923	0.898	0.881	0.912	0.893	0.891	0.900	0.857	0.915
Han		Over all Pcc/d =0.905			Over all Pcc/d =0.923			Over all Pcc/d =0.800		
	Pcc/d	0.920	0.920	0.920	0.910	0.982	0.917	0.690	0.888	0.879
	Pd	0.904	0.904	0.904	0.912	0.872	0.903	0.899	0.862	0.918
Bla		Over all Pcc/d =0.850			Over all Pcc/d =0.886			Over all Pcc/d =0.757		
	Pcc/d	0.884	0.930	0.789	0.849	0.982	0.893	0.672	0.936	0.783
	Pd	0.890	0.944	0.898	0.933	0.872	0.879	0.900	0.883	0.910

To complete the classifier comparison, confusion matrix are computed with total $P_d = 0.9$ for all the different features and classifiers. This produces twenty-four confusion matrices. Therefore, for briefly, the results from the confusion matrices are summarized in Table 3. The Percentage of correct classification in declared targets ($P_{cc/d}$) gives a single – value measure for each feature and classifier, combination breakouts of the Pcc/d and P_d for each target type are also listed in the Table 3.

It is very clear that HNeT classifier performed best in each type of features followed by the MLP NN and finally the L_2 metric measure. All three classifiers performed well using the Rectangular, Hamming and Hanning window 2D FFT features compared to their performance using other features. HNeT achieved at top $P_{cc/d}$ measure of 92.6% and MLP NN got its best at 90.7% when it used the Hamming Window. The L_2 reached its peak at $P_{cc/d} = 85.4\%$ when using the Rectangular window.

7.0 CONCLUSION

In this study eight different features four wavelets and four FFTs, and three different classifiers are compared with each other using the COMPASE Center standard MSAR evaluation method. Overall, the best results were achieved using the Hamming FFT but with Hanning and Rectangular results relatively close. The Reverse biorthogonal wavelet does show some promise with respect to the BTR-70 where only single vehicle is available, instead of three, for the target type. Further study is needed to determine if this feature set might be useful for identification purposes of individual vehicles within target type.

REFERENCE

1. D A Giglio, ed., Algorithms for Synthetic Aperture Radar Imagery I & II, Proceedings of SPIE, 1994 & 1995.
2. E G Zelnio and R J Douglass, ed., Algorithms for Synthetic Aperture Radar Imagery III, Proceedings of SPIE, 1996.
3. E G Zelnio, ed., Algorithms for Synthetic Aperture Radar Imagery IV - IX, Proceedings of SPIE, 1997 - 2003.
4. Chen-Pang,Y., Choongyeun, C., and Jeffrey, S.H., "Toward target recognition from synthetic aperture radar imagery using electromagnetics-based signatures", *The International Society for Optical Engineering*, **Vol. 42**, 2129-2149,2003.
5. Sandirasegaram, N.M. (2002). Automatic Target Recognition in SAR Imagery using a MLP Neural Network. (DRDC Ottawa TM 2002-120). Defence R&D Canada, Ottawa.
6. English, R.A. (2001). Automatic Target Recognition Using HNeT. (DREO TM 2001-080). Defence Research Establishment Ottawa.
7. Huether, B., Kempf, T. and Çetin, M.,"A Fast Hybrid Approach for SAR Classification", *European Conference on Synthetic Aperture Radar*, Ulm, Germany, 2004.
8. Zhao Q., Principe J., Brennan V., Xu D., Wang Z, "Synthetic Aperture Radar Automatic Target Recognition with Three Strategies of Learning and Representation", *IEEE Transactions on Aerospace and Electronic Systems*, 1999.
9. Achim, A. and Tsakalides, P. and Bezerianos, A., "SAR image denoising via Bayesian wavelet shrinkage based on heavy-tailed modeling", *IEEE Transactions on Geoscience and Remote Sensing*, **41(8)**, 1773-1784,2003.
10. Bhattacharya, U., Das, T.K., and Chaudhuri, B. B.,"A Cascaded Scheme for Recognition of Handprinted Numerals", *Indian Conference on Computer Vision, Graphics and Image Processing : ICVGIP 2002*, 2002.
11. Marinai, S., Gori, M. and Soda, G., "Artificial Neural Networks for Document Analysis and Recognition", *IEEE Transactions on Pattern Analysis and Machine Intelligence*, **27(1)**, 23-35, 2005

12. Chiang, J., and Paul, G., "Recognition of Handprinted Numerals in VISA Card Application Forms", *Machine Vision and Application*, 10, 144-149, 1997.
13. Costa M.C.A., and Ebecken, N. F. F. (2004), Data Mining High Performance Computing Using Neural Networks (online) http://clusterminer.nacad.ufrj.br/TechReport/RT08.pdf (February 15, 2005).
14. Bengio, S. and Bengio, Y., "Modeling High – Dimensional Discrete Data with Multi-Layer Neural Networks", *IEEE Transaction on Neural Networks special issue on data mining and knowledge discovery*, **11(3)**, 550-557, 2000.
15. Principe, J.C., Kim, M., and Fisher, J., "Target discrimination in synthetic aperture radar (SAR) using artificial neural networks", *Transactions on Image Processing*, **7(8)**, 1136-1149, 1998.
16. Pace, P., Sutherland, J. "Detection, recognition, identification and tracking of military vehicles using biomimetic intelligence", Automatic Target Recognition XI - SPIE, 326-338, Orlando, 2001.
17. HNeT2000 Application Development System User's Guide, Artificial Neural Devices Corporation. (2000).
18. (online) Artificial Neural Devices Corporation. http://www.andcorporation.com/applications.html (February 14, 2005).
19. Dudley, B. T. (April 04,2004). I-Cube Face Recognition Solutions For Stadium. (Online) I-Cube (Integrated Intelligent Imaging). http://www.i-cube.co.za/pdfs/I-Cube%20stadium%20biometric%20solution.pdf (February 15, 2005).
20. (March 12, 2002). Face recognition comes of age. (online) AcSys Biometrics Corp. http://www.twtw.ca/Portfolio/Acsys/FaceRecComesOfAge.pdf (February 12, 2005).
21. English, R.A., Rawlinson, S.J. and Sandirasegaram, N.M. (2002). Development of and ATR Workbench: Implementing a single-user interface for automating target recognition processes. DRDC Ottawa TR 2002-155. Defence R&D Canada - Ottawa.
22. Arkin, E.M., Chew, L.P., Huttenlocher, D.P., Kedem, K., and Mitchell, J.S., "An efficiently computable metric for comparing polygonal shapes". *IEEE Transactions on Pattern Analysis and Machine Intelligence*, **13**, 209-216, 1991.
23. Korfhage. R.R.. "Theoretical Measure in P/Q Document Spaces", *Proceedings of the 8th Annual International ACM SIGIR Conference on Research and Devlopment in Information Retrieval*, 33-40, Montreal, 1985.
24. (Oct 19 2004) MSTAR OVERVIEW, (online) Sensor Data Management System, https://www.sdms.afrl.af.mil/datasets/mstar/ (February 18, 2005)
25. Ross, T.D., and Mossing, J.C., "The MSTAR Evaluation Methodology", *Algorithms for SAR Imagery VI – SPIE*, 705 - 715, Orlando, 1999.
26. Ross, T.D., Velten, V., Mossing, J.C., Worrell, S., and Bryant, M.. "Standard SAR ATR Evaluation Experiments using the MSTAR Public Release Data Set", *Algorithms for Synthetic Aperture Radar Imagery V - SPIE*, 566-573. Orlando, 1998.
27. O'Sullivan, J.A., DeVore, M.D., Kedia, V.," Performance Analysis of ATR from SAR Imagery", *Proceedings of the 33rd Annual Conference on Information Science and Systems*, Baltimore, MD, 1999.
28. Joan, L. (2004). 4F8 Image Processing and Image Coding Image Processing Handout 4. (online) University of Cambridge. http://www-sigproc.eng.cam.ac.uk/~jl/imageproc/index.php (February 16, 2005).
29. Pratt, W.K., *Digital Image Processing* (Second Edition), John Wiley & Sons, Inc., Toronto, 1991.
30. Jackson, L.B., *Digital Filters and Singal Processing* (Second Edition), Kluwer Academic Publishers, Boston, 1989.
31. Romberg, J., Choi, H., and Baraniuk, R., "Bayesian Tree-Structured Image Modeling Using Wavelet-Domain Hidden Markov Models", *IEEE Transactions on image processing*, **10(7)**, 1056-1068, 2001.

32. Kopp, M., "Lossless Wavelet Based Image Compression with Adaptive 2D Decomposition", (TR-186-2-95-11), Institute of Computer Graphics and Algorithms, Vienna University of Technology, Austria, 1995.
33. Kotteri, K. A. Optimal, "Multiplierless Implementations of the Discrete Wavelet Transform for Image Compression Applications", Master's Thesis, Electrical and Computer Engineering, Virginia Polytechnic Institute and State University, April 2004.
34. Mallat, S., "A Theory for Multiresolution Signal Decomposition: The Wavelet Representation", *IEEE Transactions on pattern analysis and machine intelligence*, **11(7)**, 674-693, 1989.
35. Zhang, B., Zhang, H., and Ge, S., "Face Recognition by Applying Wavelet Subband Representation and Kernel Associative Memories", *IEEE Transactions on Neural Networks*, **15(1)**, 166-177, 2004
36. M. Misiti,Y. Misiti,G. Oppenheim and J.-M. Poggi (2002). "Wavelet Toolbox: for use with MATLAB," version 2.2, The Mathworks Inc., http://www.mathworks.com/access/helpdesk/help/pdf_doc/wavelet/wavelet_ug.pdf (February 18, 2005).
37. HNeT2000 Application Development System User's Guide, Artificial Neural Devices Corporation. (2000).
38. (online) Artificial Neural Devices Corporation. http://www.andcorporation.com/applications.html (February 18, 2004).
39. DRDC Ottawa TR 2002-155. Defence R&D Canada - Ottawa.
40. Klepko, R., "The Holographic Neural Network: Performance comparison with other Neural Networks", (DREO TN 91-18), Defence Research Establishments Ottawa, 1991.
41. Sutherland, J.G., "A Holographic Model of Memory, Learning and Expression", *International Journal of Neural System*, **1(3)**, 259-267, 1990.